

A modified Q4/Q4 element for topology optimization

Glaucio H. Paulino · Chau H. Le

Received: 3 November 2005 / Revised: 19 November 2007 / Accepted: 21 December 2007 / Published online: 31 October 2008
© Springer-Verlag 2008

Abstract Design variable and displacement fields are distinct. Thus, their respective material and finite element meshes may also be distinct, as well as their actual location of nodes for the two fields. The proposed Q4/Q4M element possesses design variable nodes and displacement nodes which are not coincident. The element has been implemented using different approaches, including continuous approximation of material distribution and nodal approaches. The results obtained demonstrate that the element is effective in generating structural topologies with high resolution. From a numerical point of view, mesh independent solutions can be obtained by means of projection.

Keywords Topology optimization · Node-based design variables · Material mesh · Displacement mesh · Q4/U · Q4/Q4 · Q4/Q4M

1 Introduction

Several approaches based on nodal design variables have been developed (Rahmatalla and Swan 2004; Matsui and Terada 2004; Guest et al. 2004). According to these approaches, values of material density at nodes are considered as design variables, and traditional element material densities are obtained from nodal values with projection (or interpolation) schemes. In essence,

the introduction of nodal design variables and projection schemes in those approaches provides natural control over the local gradient of material densities. As a consequence, the checkerboard problem Diaz and Sigmund 1995 is either eliminated or alleviated. Recently, Rahmatalla and Swan (2004) have shown a number of options for element-wise interpolation of displacement and material density fields. However, the choice of nodal design variable location has not been fully explored, and thus the purpose of this paper is to investigate a new arrangement of nodal design variables for the displacement-based bilinear quadrilateral element. In this paper, we propose and investigate another option for quadrilateral elements—the Q4/Q4M (i.e., modified Q4/Q4). This element has four nodal design variables located at the midpoints of the four edges of the quadrilateral. This option for the locations of nodal design variables provides a higher resolution for topological results without increasing mesh refinement for displacement discretization.

Guest et al. (2004) proposed an approach to achieve minimum length scale and checkerboard-free property by introducing nodal design variables and projection schemes (for convenience, it is referred to as the nodal approach in this paper). According to this approach, values of material density at nodes are considered as design variables, which are updated by the optimization module. Material density is assumed to be uniform for each displacement-based element. Element material densities are derived from nodal design variables using projection schemes and are used to determine element stiffness matrices for the finite element analysis module. This is in contrast to the traditional element-based implementation in which element material densities are also the design variables that are directly updated by

G. H. Paulino (✉) · C. H. Le
Department of Civil and Environmental Engineering,
University of Illinois at Urbana–Champaign,
Newmark Laboratory, 205 North Mathews Avenue,
Urbana, IL 61801, USA
e-mail: paulino@uiuc.edu

the optimization module. The introduction of nodal design variables as representations of element material densities and projection schemes in the nodal approach results in an implicit restriction on local gradient of element material densities. Thus, it avoids checkerboard patterns in the solution space and includes a minimum length scale (desirable feature).

Implicit restriction on local gradient of material density is also a feature of the continuous approximation of material distribution (CAMD) approach in which the material density field is assumed continuous within and between elements. Continuous element material density is interpolated from nodal values, which are design variables, using shape functions. Continuity of the material density field prevents adjacency between solid and void elements. Change in material density from solid to void must occur over at least one element, which means that checkerboard patterns are not favored.

Both approaches described above (i.e., the nodal design variables with projection scheme and the CAMD approach) claim checkerboard-free property naturally without additional constraints or filtering techniques. This feature is believed to come from the implicit restriction on gradient of material density field common in both approaches. The key to the above restriction is the introduction of nodal design variables and projection/interpolation schemes. In a regular Q4/Q4 element where nodal design variables are located at four vertices of the quadrilateral, each design variable contributes equally to the material density of four surrounding elements. However, it is sufficient to prevent checkerboard patterns by controlling the gradient of material density between only two elements sharing a common edge. The Q4/Q4M element proposed in this paper does exactly that; thus, it preserves the checkerboard-free property while allowing higher resolution for the solution (i.e., solutions with well-defined structural members).

The implementation of the Q4/Q4M element also highlights the distinction between design variable space and displacement space. In the paper describing the so-called nodal approach (Guest et al. 2004), nodal design variables are deemed at the same locations with nodes of Q4 elements. Likewise, in the “selected options” for the quadrilateral elements provided by Rahmatalla and Swan (2004), elements for material density approximation are either embedded or coincident with elements for displacement approximation. For the CAMD options in that paper (Rahmatalla and Swan 2004), nodal design variables are always considered at the locations of displacement nodes. However, design variable and displacement fields are two distinct fields. Therefore,

the material and finite element meshes as well as locations of nodes for the two fields may be independent, although using the same mesh for both fields may also be a good choice. In the implementation of the Q4/Q4M element in this paper, design variable nodes and displacement nodes are not coincident. Furthermore, the standard finite element mesh and the material density mesh are different in the CAMD implementation. We note that the decoupling of topology definition and the finite element mesh was also an important feature of an approach using topology definition function by de Ruiter and van Keulen (2004).

Rahmatalla and Swan (2004) reported instabilities in their implementation of the Q4/Q4 element as “layering” and “islanding” phenomena. Those instabilities were mathematically addressed by Jog and Haber (1996) (for the Q4/Q4 element). Similarly, we also noticed numerical instabilities in the implementation of the Q4/Q4M element using the CAMD approach. In the present paper, we apply a heuristic averaging of energy densities at Gauss points of each element to avoid the above instabilities. This internal averaging does not cause additional “gray” areas, nor does it lead to lower resolution of resulting structures. This feature will be discussed later in this paper.

The remainder of this paper is organized as follows. Section 2 describes the geometry and implementation of the Q4/Q4M element. Section 3 discusses numerical instability of the CAMD approach and the internal averaging technique. Section 4 lists the options that are implemented for result comparison. Section 5 shows and compares results of an example problem. Finally, conclusions are given in Section 7.

2 The Q4/Q4M element: implementation aspects

The Q4/Q4M element uses a regular Q4 element for the displacement field and four nodes located at midpoints of the Q4 element edges to represent the material density field. Figure 1 compares the proposed Q4/Q4M element with the Q4/Q4 element and the standard Q4/U (Q4 with uniform material density) element.

For simplicity and clarity, standard square meshes as shown in Fig. 3 are considered for all implementations in this paper. The Q4/Q4M element is implemented according to the following two variations:

1. Uniform material density inside each element, and
2. Variable material density inside each element.

The first implementation is similar to the nodal approach, and the second one is in accordance with the CAMD approach. In this paper, we use the solid

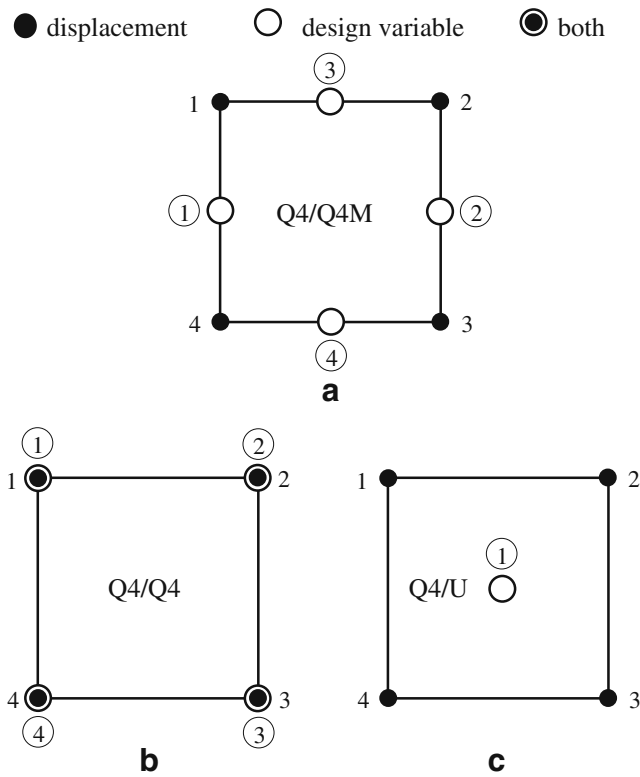


Fig. 1 Element-wise interpolation of displacement and design variable: **a** Q4/Q4M, **b** Q4/Q4, **c** Q4/U

isotropic material with penalization (SIMP) (Rozvany et al. 1992; Bendsoe 1989; Bendsoe and Sigmund 1999) model for interpolation of the stiffness tensor of intermediate material density. Below are some details of the two implementations.

2.1 Uniform material density inside each element

Implementation for the first case, in which element material density is considered as uniform, is briefly described below. In this case, the design variables are better referred to as edge design variables. The projection from edge design variables to element density (ρ^e) is a simple averaging process:

$$\rho^e = \frac{(\rho_1^e + \rho_2^e + \rho_3^e + \rho_4^e)}{4} \tag{1}$$

where ρ_i^e denotes the design variable at edge i (see Fig. 1) of the element e . Sensitivities of total material volume and mean compliance (c) with respect to design variables are also simple and cheap to compute:

$$\frac{\partial v}{\partial \rho_j} = \frac{1}{4} \text{ for exterior nodes;} \tag{2}$$

$$\frac{\partial v}{\partial \rho_j} = \frac{1}{2} \text{ for interior nodes} \tag{3}$$

and

$$\frac{\partial c}{\partial \rho_j} = - \sum_{e=1}^n \frac{1}{4} P \left(\frac{\rho_1^e + \rho_2^e + \rho_3^e + \rho_4^e}{4} \right)^{(p-1)} (\mathbf{U}^e)^T \mathbf{K}^e \mathbf{U}^e \tag{4}$$

where n is the number of elements associated with edge j ($n = 1$ for exterior edges and $n = 2$ for interior edges), p is the penalization parameter in the SIMP model, and \mathbf{U}^e and \mathbf{K}^e are displacement vector and element stiffness matrix of element e , respectively.

The above implementation aims to generate high resolution for topological results. However, it does not feature minimum length scale or solve the problem of mesh dependency. Note that high resolution for the final topology has been the objective of various methods, which attempt to suppress checkerboard patterns and direct corner contact (Pomezanski et al. 2005; Poulsen 2002, 2003; Sigmund and Petersson 1998).

According to the above implementation, each design variable controls material density in two elements instead of four as in the case of the Q4/Q4. This feature is believed to yield higher resolution for topological results. When the topology is represented by nodal values and projection schemes, the design space is constructed from patches of elements (see Fig. 2). In the case of the Q4/Q4, each patch contains four elements that share a common vertex. In the case of the Q4/Q4M, each patch contains two elements that share a common edge. Material density in each patch is represented by one design variable. The smaller the patches, the higher the resolution obtained. As patches of Q4/Q4M element are smaller, they are capable of providing higher resolution for topological results.

2.2 Variable material density inside each element

Implementation for the second case, in which material density is considered as a continuous variable within and between elements, requires interpolation of material density by shape functions. Besides the relevance of this topic by itself, it is also important for the topology design of functionally graded materials, which possess continuous variation of material properties inside the design domain (Paulino and Silva 2005; Paulino et al. 2005). These materials have been modeled by graded finite elements (Kim and Paulino 2002) in which the material properties are interpolated by means of the element shape functions. The concept of graded elements is especially useful for the CAMD approach.

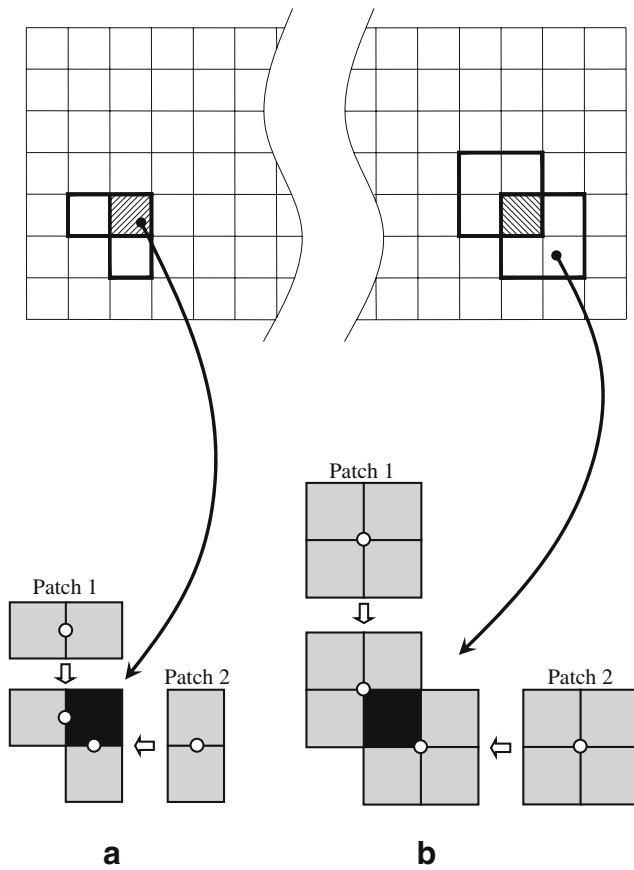


Fig. 2 Construction of design space from patches: **a** patches of Q4/Q4M elements, **b** patches of Q4/Q4 elements

Element stiffness matrices are obtained by integrating their contributions over the element subdomain. Material property matrix (\mathbf{D}) is dependent on the material density and, therefore, is variable. In common practice, numerical (e.g., Gauss) quadrature is used for the numerical integration. The integration is reduced to the evaluation and summation of the stiffness matrix integrand at Gauss points. The interpolation of

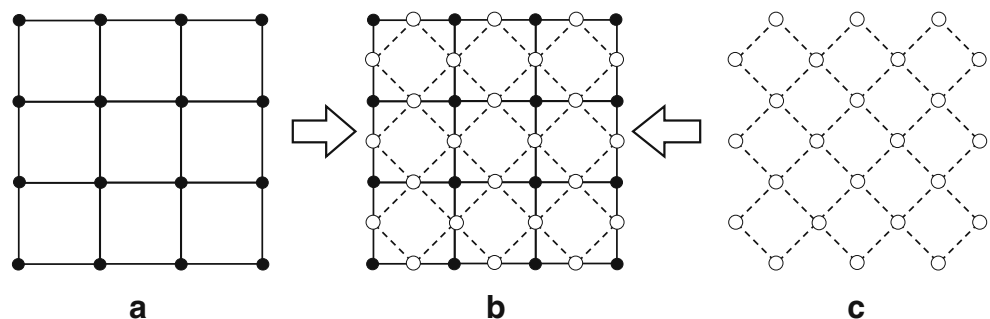
material density is reduced to a projection of nodal design variables to Gauss points.

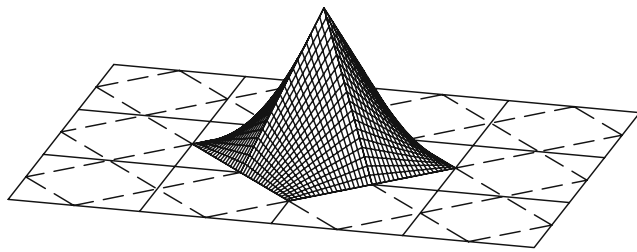
Before going into detail of the shape functions for the material density of the Q4/Q4M, it is important to distinguish the two element meshes involved in topology optimization with continuous approximation of material distribution. The first mesh is the one used to discretize displacement field (assume that displacement based finite elements are used). This mesh is referred to as *displacement mesh* (finite element mesh) and consists of *displacement elements* (finite elements). The second mesh is the one used to discretize material density and will be referred to as *material mesh* consisting of *material elements*. These two meshes are two distinct entities, and more importantly, they are not necessarily coincident, as will be shown later.

For the case of the Q4/Q4M, *displacement elements* and *material elements* may be of the same type. However, shape functions for *material elements* and *displacement elements* are not the same, as locations of nodes in the two types of elements are different. For displacement interpolation, well established bilinear shape functions for the Q4 conforming element are used. Alternatively, the material density may be interpolated using nonconforming shape functions as described by Douglas et al. (1999) and used by Jang et al. (2003). However, nonconforming shape functions can lead to negative material density and severe numerical instabilities. Therefore, another approximation scheme is used and described as follows.

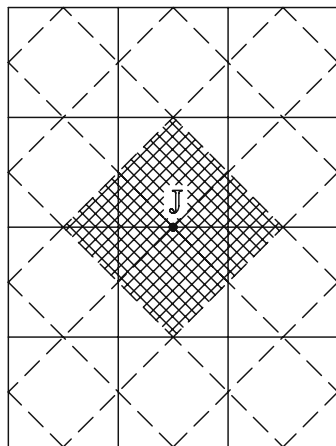
The *material mesh* is chosen differently from the *displacement mesh*. Figure 3 illustrates the *displacement mesh* and *material mesh* separately and how they are superposed. The material mesh also contains Q4 elements, but they are rotated by 45°. The area of each element in the material mesh is half the area of each element in the displacement mesh. Thus, with the same displacement mesh, the resolution of the solution generated with Q4/Q4M elements will be higher

Fig. 3 Composition of displacement and material meshes: **a** displacement mesh, **b** resulting superposed meshes, **c** material mesh





Global shape function associated with node J



Plan view for location of node J

Fig. 4 Shape function for material density interpolation

than that generated by Q4/Q4 elements. Because the *material mesh* consists of Q4 elements, the material density can be interpolated using regular bilinear shape functions. Figure 4 illustrates the shape function corresponding to one design variable.

With the above approximation for material density, sensitivities of total material volume are similar to those given for the nodal approach.

$$\frac{\partial v}{\partial \rho_i} = \frac{1}{4} \text{ for exterior nodes} \tag{5}$$

$$\frac{\partial v}{\partial \rho_i} = \frac{1}{2} \text{ for interior nodes} \tag{6}$$

Calculation of stiffness matrices for displacement elements and sensitivity of mean compliance with respect to design variables is not trivial, as each displacement is overlapped with several material elements. Below is the calculation of sensitivity of compliance (c) with respect to one nodal design variable (ρ_1 ; see Fig. 5):

$$\frac{\partial c}{\partial \rho_1} = \left(\frac{\partial c}{\partial \rho_1} \right)_1 + \left(\frac{\partial c}{\partial \rho_1} \right)_2 \tag{7}$$

where $(\partial c / \partial \rho_1)_1$ and $(\partial c / \partial \rho_1)_2$ are contributions from finite elements 1 and 2, respectively, which are given by:

$$\begin{aligned} \left(\frac{\partial c}{\partial \rho_1} \right)_1 = & -(\mathbf{U}_1)^T \left\{ \mathbf{K}_1 \phi_3(A_1) p [\rho_6 \phi_1(A_1) + \rho_2 \phi_2(A_1) \right. \\ & \left. + \rho_1 \phi_3(A_1) + \rho_5 \phi_4(A_1)]^{p-1} \right. \\ & \left. + \mathbf{K}_4 \phi_1(A_4) p [\rho_1 \phi_1(A_4) + \rho_4 \phi_2(A_4) + \rho_{11} \phi_3(A_4) \right. \\ & \left. + \rho_{12} \phi_4(A_4)]^{(p-1)} \right\} \mathbf{U}_1 \tag{8} \end{aligned}$$

$$\begin{aligned} \left(\frac{\partial c}{\partial \rho_1} \right)_2 = & -(\mathbf{U}_2)^T \left\{ \mathbf{K}_2 \phi_3(A_2) p [\rho_6 \phi_1(A_2) + \rho_2 \phi_2(A_2) \right. \\ & \left. + \rho_1 \phi_3(A_2) + \rho_5 \phi_4(A_2)]^{p-1} \right. \\ & \left. + \mathbf{K}_3 \phi_1(A_3) p [\rho_1 \phi_1(A_3) + \rho_4 \phi_2(A_3) + \rho_{11} \phi_3(A_3) \right. \\ & \left. + \rho_{12} \phi_4(A_3)]^{(p-1)} \right\} \mathbf{U}_2 \tag{9} \end{aligned}$$

where \mathbf{K}_1 , \mathbf{K}_2 , \mathbf{K}_3 , and \mathbf{K}_4 are values of the integrand of the stiffness matrix at the selected four Gauss points; ϕ_1 , ϕ_2 , ϕ_3 , and ϕ_4 are four standard shape functions for the bilinear quadrilateral element (Cook et al. 2002); \mathbf{U}_1 and \mathbf{U}_2 are the nodal displacements for elements 1 and 2, respectively; and “A” denotes coordinates of Gauss points with respect to the material mesh: $A_1 = (-2 + 2/\sqrt{3}, 0)$; $A_2 = (0, -2 + 2/\sqrt{3})$; $A_3 = (+2 - 2/\sqrt{3}, 0)$; $A_4 = (0, +2 - 2/\sqrt{3})$. Notice that the Gauss points employed for the calculation of sensitivity are the ones

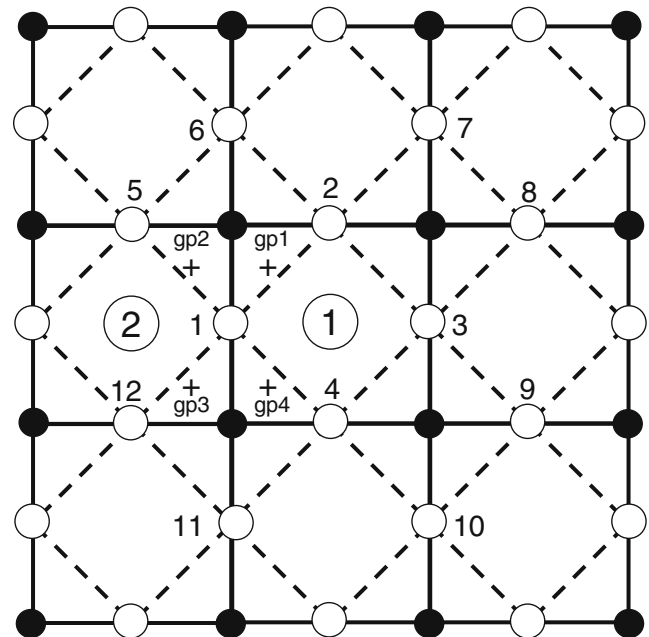


Fig. 5 Illustration of the calculation of sensitivity

at which material densities are effected by the nodal design variable ρ_1 . Those Gauss points belong to elements 1 and 2, as illustrated by Fig. 5.

However, as mentioned above, the integration for element stiffness matrices is practically the evaluation and summation of the integrand at Gauss points, and the interpolation process is essentially the projection of design variables to Gauss points. Therefore, we adopt a simplified procedure in which four Gauss points are considered for each displacement element and the value of material density at each Gauss point is taken as the average of the two design variables adjacent to it. According to the simplified procedure, the compliance sensitivities are as follows:

$$\left(\frac{\partial c}{\partial \rho_1}\right)_1 = -(\mathbf{U}_1)^T \frac{1}{2} \left[\mathbf{K}_1 p \left(\frac{\rho_1 + \rho_2}{2}\right)^{p-1} + \mathbf{K}_4 p \left(\frac{\rho_4 + \rho_1}{2}\right)^{p-1} \right] \mathbf{U}_1 \quad (10)$$

$$\left(\frac{\partial c}{\partial \rho_1}\right)_2 = -(\mathbf{U}_2)^T \frac{1}{2} \left[\mathbf{K}_2 p \left(\frac{\rho_1 + \rho_5}{2}\right)^{p-1} + \mathbf{K}_3 p \left(\frac{\rho_{12} + \rho_1}{2}\right)^{p-1} \right] \mathbf{U}_2. \quad (11)$$

3 Numerical instabilities of CAMD approach and the internal averaging technique

Matsui and Terada (2004) claimed that the CAMD approach is a checkerboard-free approach. However, Rahmatalla and Swan (2004) have reported other forms of numerical instabilities and called them “islanding” and “layering” phenomena. We also encountered the same phenomena while reproducing results of the CAMD approach with the Q4/Q4 and Q4/Q4M elements. These forms of numerical instabilities reduce the quality of topological results. To compare the Q4/Q4 and the Q4/Q4M elements in their best capacities, we introduced a simple but effective treatment called “internal averaging technique.” This treatment is similar to the filter of sensitivities (Sigmund 2001). It removes the “islanding” and “layering” phenomena while maintaining the resolution of topological results and avoiding additional “gray” areas. The technique is described in the following paragraph.

In Section 2.2, total design sensitivity with respect to one nodal design variable (e.g., ρ_1 in Fig. 5) is calculated as sum of the contributions of two adjacent elements (i.e., elements 1 and 2). The contributions of each element (e.g., element 1) for its four nodes (i.e., nodes 1, 2, 3, and 4) are different and are calculated by

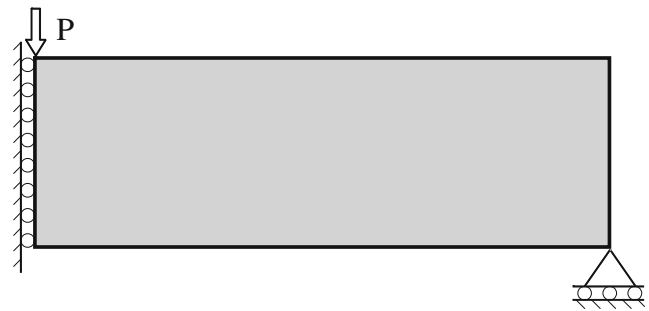


Fig. 6 Configuration for half of the MBB beam with aspect ratio length/width = 6:1 (for the entire beam)

Gauss quadrature. The averaging process takes place at this step. The contributions of each element to the design sensitivities with respect to its four nodal design variables are averaged out before being added to the total design sensitivities. The term $(\partial c/\partial \rho_1)_1$ then becomes:

$$\left(\frac{\partial c}{\partial \rho_1}\right)_1 = -(\mathbf{U}^1)^T \frac{1}{4} \left[\mathbf{K}_1 p \left(\frac{\rho_1 + \rho_2}{2}\right)^{p-1} + \mathbf{K}_2 p \left(\frac{\rho_2 + \rho_3}{2}\right)^{p-1} + \mathbf{K}_3 p \left(\frac{\rho_3 + \rho_4}{2}\right)^{p-1} + \mathbf{K}_4 p \left(\frac{\rho_4 + \rho_1}{2}\right)^{p-1} \right] \mathbf{U}^1. \quad (12)$$

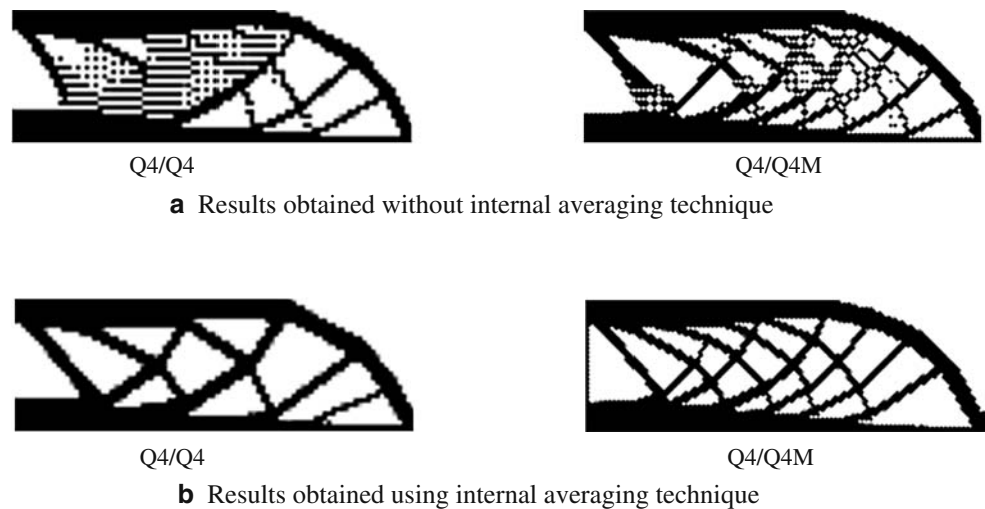
The above averaging process acts internally within each element and does not reduce the resolution of topological results.

To demonstrate the effectiveness of the “internal averaging technique,” we consider the so-called Messerschmitt–Bolkow–Blohm (MBB; e.g., Olhoff et al. 1991) beam example of Fig. 6. The beam topologies are obtained according to a minimum compliance objective. We contrast in Fig. 7 the results obtained without (Fig. 7a) and with (Fig. 7b) internal averaging. The results of Fig. 7a exhibit “islanding” and “layering” (undesirable features), while the results of Fig. 7b do not.

4 Computational implementations

To have an equitable assessment of the performance of the new Q4/Q4M element, the well-established minimum compliance problem is chosen (see, for example, Bendsoe and Sigmund 2003). Various elements and approaches (including the traditional element-based method with filtering techniques) are implemented—see Table 1. In all implementations, the original ver-

Fig. 7 Effectiveness of the internal averaging technique (discretization level: 90×30 ; volume constraint = 50%)



sion of the optimality criteria method as described in Bendsoe and Sigmund (2003); Sigmund (2001) is used as an optimizer.

5 Demonstrative examples

Variations of the MBB beam (Olhoff et al. 1991) are solved using various elements and approaches. Results are contrasted to facilitate the evaluation. Volume constraints are taken as 50%. Stiffness tensor of intermediate material density is interpolated according to the SIMP method. Continuation technique is used in all examples to achieve high resolution of the topology. Note that the same continuation technique is used in all cases: penalization is set to 1 at the beginning of the iteration process and increased by 0.2 when the solution is sufficiently converged, until final penalization is reached. Poisson's ratio is chosen as 0.3. Symmetry of the MBB beam is employed, and only half of the beam is modeled. The beam has an aspect ratio of 6:1 corresponding to length over height. Three mesh refinement levels (45×15 , 90×30 , and 150×50) are adopted for each approach. Figure 6 shows the configuration for half of the MBB beam (Fig. 7).

The first batch of results is from the class of approaches that assume uniform material density within each displacement element. Those approaches include

element-based approach (Q4/U), nodal approach using Q4/Q4, and nodal approach using Q4/Q4M. We use the 99-line Matlab code written by Sigmund (2001) for the Q4/U option. A filtering radius of 1.2 is used, which is sufficient to suppress checkerboard patterns in the solution. For the nodal approach using Q4/Q4, length scale control parameter r_{\min} is set to 1.0 so that minimum possible member size is achieved. It is clear from the results that the new Q4/Q4M element generates structures with more number of structural members that are finer. In other words, the resolution of the solution is higher. The results are in agreement with the prediction in Section 2 about the resolution of the new Q4/Q4M element (see Fig. 8).

The second batch of results is obtained with CAMD approach using Q4/Q4M and Q4/Q4 elements. Each type of element is also implemented with three mesh refinement levels (45×15 , 90×30 , and 150×50). The internal averaging technique, as described in Section 3, has been applied to the CAMD implementation of both the Q4/Q4 and the Q4/Q4M. Again, higher resolutions for final structures are obtained with the Q4/Q4M (see Fig. 9). Actually, we can notice from Fig. 9 that results in items (c) and (e) are almost the same. That indicates a mesh resolution of 90×30 using the new Q4/Q4M which is equivalent to a mesh resolution of 150×50 using the standard Q4/Q4 element in terms of ability to generate comparable and fine structural patterns.

The numerical optimization results shown above agree well with the analytical solution derived by Lewinski et al. (1994). The vertical bars in several results (Figs. 8f and h and 9c and e) may bring concerns about the correctness of the implementation because of the following reasons. First, the vertical bars are not present in all results. Second, this type of vertical bars

Table 1 Implemented options

Assumptions	Elements	Approaches
Uniform element density (Fig. 8)	Q4/U	Sensitivity filter
	Q4/Q4	Nodal approach
	Q4/Q4M	Nodal approach
Variable element density (Fig. 9)	Q4/Q4	CAMD approach
	Q4/Q4M	CAMD approach

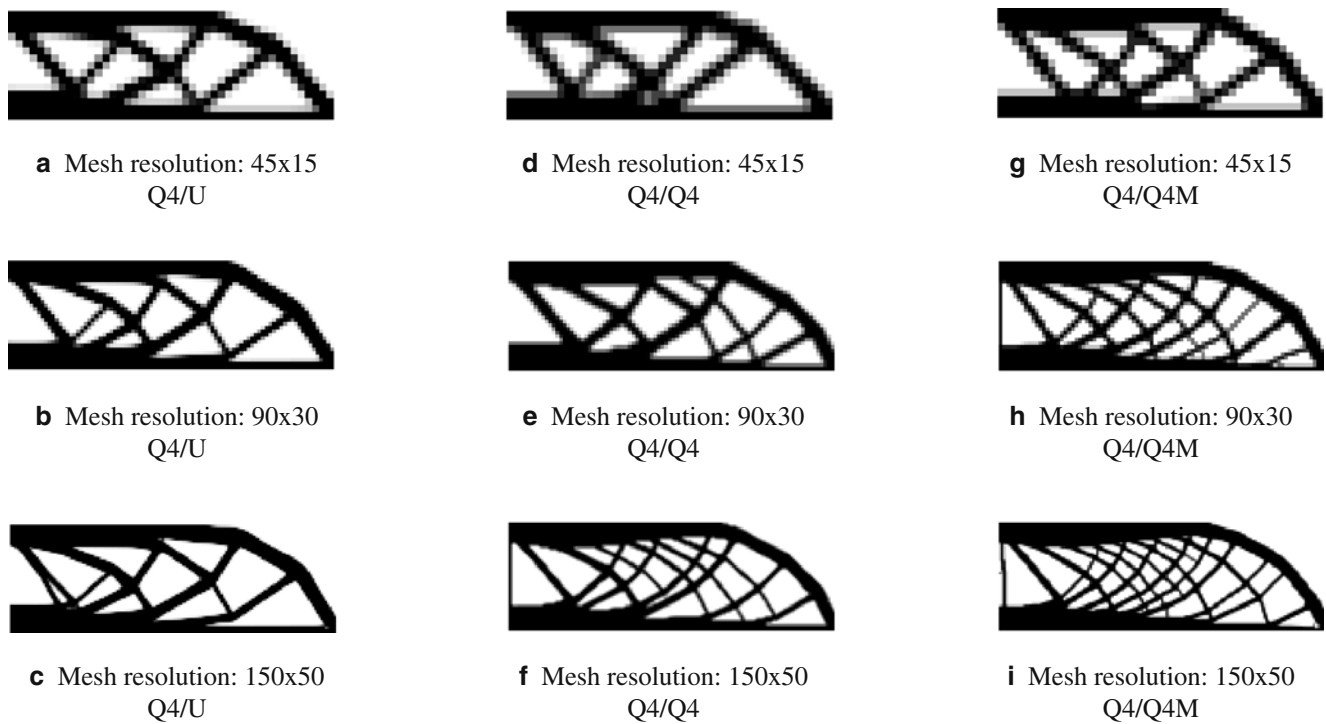
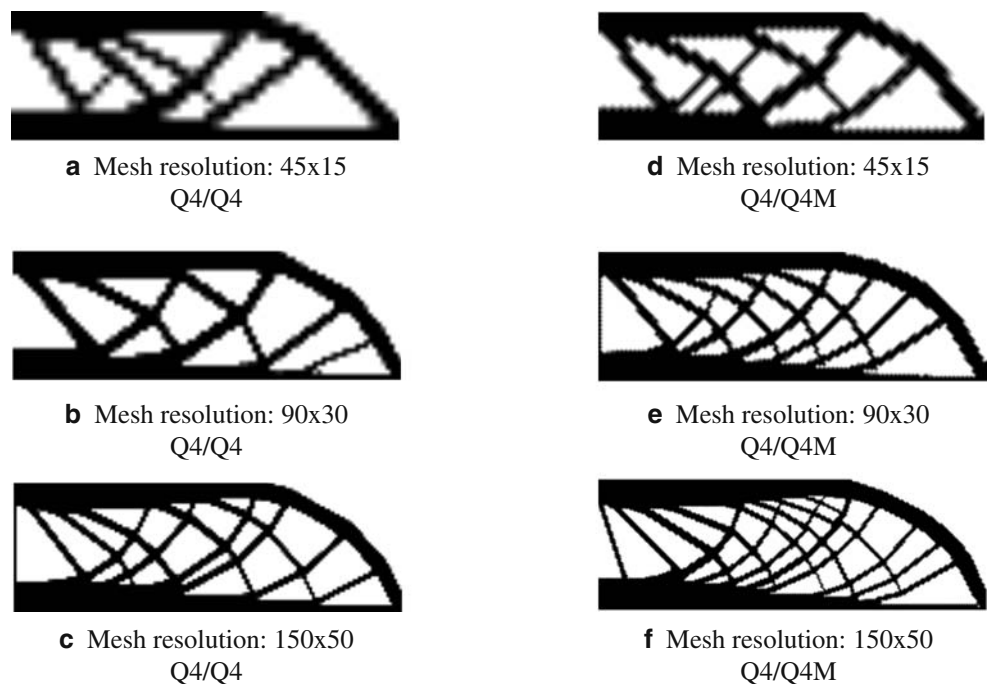


Fig. 8 Solutions for the MBB beam: Uniform material density is assumed within each element. **a–c** Solution with SIMP approach (Q4/U) and filtering radius of 1.2; **d–f** solution with Q4/Q4 element and nodal approach; **g–i** solution with Q4/Q4M and nodal approach

have zero internal forces for truss structures and are redundant. However, topological results are mesh dependent in general. Different results may be obtained with different approaches and mesh sizes. The structures in our results are not purely hinged trusses, and

internal forces in the vertical bars are present. Thus, the vertical bars are not redundant, and their presence in several results is reasonable. We also noticed similar vertical bars in the results provided by Rahmatalla and Swan (2004).

Fig. 9 Solutions for the MBB beam using CAMD approach with the internal averaging technique (see Section 2): **a–c** solution with Q4/Q4, **d–f** solution with Q4/Q4M



We noticed that very high resolution solution was obtained early in the literature (Rozvany et al. 1992; Zhou and Rozvany 1991) using SIMP method. The results are not compared directly in this paper because the problem setting and checkerboard prevention technique used in the referenced publications are not available to us.

6 Mesh-dependency problem

Both the Q4/Q4M element, as well as the Q4/Q4 element, do not provide mesh independency. To obtain mesh-independent solutions, a length scale is introduced. We choose to apply a variation of the filter of densities described by Bruns and Tortorelli (2001), which has some similarity to the approach by Guest et al. (2004). However, the former authors employed element design variables, while the latter ones employed nodal design variables. Figure 10 explains our implementation of the technique with the Q4/Q4M element. In our implementation, design variables are located at center of elements, and the density measures are nodal densities. In previous sections, we show that the Q4/Q4M element provides higher resolution (finer structural patterns) for the solutions. In this section, the results have a minimum length scale, so we obtained mesh-independent solutions. However, as the material

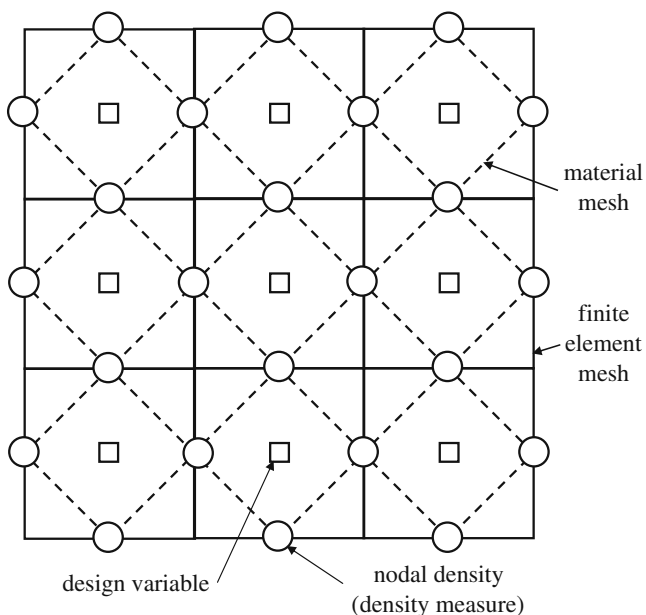
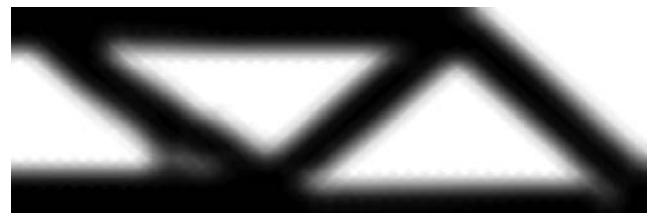


Fig. 10 Locations of design variables and nodal densities used for the density filtering technique



a Mesh resolution: 45x15 Q4/Q4M elements



b Mesh resolution: 90x30 Q4/Q4M elements



c Mesh resolution: 150x50 Q4/Q4M elements

Fig. 11 Mesh-independent solutions using the filter of densities (Bruns and Tortorelli 2001) with the Q4/Q4M element. Minimum member size is 20% of beam height. Problem configuration is similar to Fig. 9

mesh for the Q4/Q4M is finer, the boundaries can be better defined. Figure 11 shows the results obtained using the Q4/Q4M element with a minimum length scale. The configuration of the design domain is the same as the examples in Section 5. The minimum member size (including “gray” areas) is 1/5 of the beam height.

7 Conclusions

In this paper, we propose a new arrangement of nodal design variables for the displacement-based Q4 element. This new option has been implemented using different approaches including CAMD and nodal approaches. In both cases, the new option proved to be more advantageous in generating higher resolution for topological results. Nevertheless, options for arrangement of nodal design variables are not exhausted, especially when considering different meshes for displacement field and material distribution field.

While implementing the CAMD approach for the Q4/Q4M element, we also encountered the numerical

instabilities in the form of “layering” and “islanding,” as reported by Rahmatalla and Swan (2004) for the Q4/Q4 element. An internal averaging technique has been applied to successfully suppress those instabilities. This technique does not require user’s input of either filtering strength or radius.

This paper has shown that dissociating the discretization of the design variable field and the primary variable field (e.g. displacement) offers advantages over the conventional approach that uses the same basic discretization for both fields. Thus the idea of decoupling the parameterization of the design field(s) and the finite element discretization of the design domain offers room for further developments in topology optimization.

Acknowledgements Support from the Center for Process Simulation and Design (CPSD) at the University of Illinois is gratefully acknowledged. The US National Science Foundation supports research in the CPSD via grant NSF DMR 01-21695. This work was funded in part by a grant from the Vietnam Education Foundation (VEF). The opinions, findings, and conclusions stated herein are those of the authors and do not necessarily reflect those of the sponsors.

References

- Bendsoe MP (1989) Optimal shape design as a material distribution problem. *Struct Multidisc Optim* 1:193–202
- Bendsoe MP, Sigmund O (1999) Material interpolation schemes in topology optimization. *Arch Appl Mech* 69:635–654
- Bendsoe MP, Sigmund O (2003) *Topology optimization: theory, methods and applications*. Springer, New York
- Bruns TE, Tortorelli DA (2001) Topology optimization of nonlinear elastic structures and compliant mechanisms. *Comput Methods Appl Mech Eng* 190:3443–3459
- Cook RD, Malkus DS, Plesha ME, Witt RJ (2002) *Concepts and applications of finite element analysis*. John Wiley & Sons Inc., New York, 96–100
- de Ruiter MJ, van Keulen F (2004) Topology optimization using a topology description function. *Struct Multidisc Optim* 26:406–416
- Diaz A, Sigmund O (1995) Checkerboard patterns in layout optimization. *Struct Multidisc Optim* 10:40–45
- Douglas Jr J, Santos JE, Sheen D, Ye X (1999) Nonconforming Galerkin methods based on quadrilateral elements for second order elliptic problems. *Model Math Anal Numer* 33:747–770
- Guest JK, Prevost JH, Belytschko T (2004) Achieving minimum length scale in topology optimization using nodal design variables and projection functions. *Int J Numer Methods Eng* 61:238–254
- Jang J, Jeong JH, Kim YY, Sheen D, Park C, Kim MN (2003) Checkerboard-free topology optimization using non-conforming finite elements. *Int J Numer Methods Eng* 57:1717–1735
- Jog CS, Haber RC (1996) Stability of finite element models for distributed-parameter optimization and topology design. *Comput Methods Appl Mech Eng* 130:203–226
- Kim JH, Paulino GH (2002) Isoparametric graded finite elements for nonhomogeneous isotropic and orthotropic materials. *ASME J Appl Mech* 69:502–514
- Lewinski T, Zhou M, Rozvany GIN (1994) Extended exact least-weight truss layouts, part II: asymmetric cantilevers. *Int J Mech Sci* 36:399–419
- Matsui K, Terada K (2004) Continuous approximation of material distribution for topology optimization. *Int J Numer Methods Eng* 59:1925–1944
- Olhoff N, Bendsoe MP, Rasmussen J (1991) On CAD-integrated structural topology and design optimization. *Comput Methods Appl Mech Eng* 89:259–279
- Paulino GH, Silva ECN (2005) Design of functionally graded structures using topology optimization. *Mat Sci Forum* 492–493:435–440
- Paulino GH, Page III, RC, Silva ECN (2005) A Java-based topology optimization program with web access: nodal design variable approach. 6th World Congress on Struct Multidisc Optim—Book of Abstracts 1471:135–135
- Pomezanski V, Querin OM, Rozvany GIN (2005) CO-SIMP: extended SIMP algorithm with direct corner contact control. *Struct Multidisc Optim* 30:164–168
- Poulsen TA (2002) A simple scheme to prevent checkerboard patterns and one-node connected hinges in topology optimization. *Struct Multidisc Optim* 24:396–399
- Poulsen TA (2003) Topology optimization in wavelet space. *Int J Numer Methods Eng* 53:567–582
- Rahmatalla SF, Swan CC (2004) A Q4/Q4 continuum structural topology optimization implementation. *Struct Multidisc Optim* 27:130–135
- Rozvany GIN, Zhou M, Birker T (1992) Generalized shape optimization without homogenization. *Struct Multidisc Optim* 4:250–252
- Sigmund O (2001) A 99 line topology optimization code written in Matlab. *Struct Multidisc Optim* 27:130–135
- Sigmund O, Petersson J (1998) Numerical instabilities in topology optimization: a survey on procedures dealing with checkerboards, mesh-dependencies and local minima. *Struct Multidisc Optim* 16:68–75
- Zhou M, Rozvany GIN (1991) The COC algorithm, part II: topological, geometrical and generalized shape optimization. *Comput Methods Appl Mech Eng* 89:309–336